

RING1B contributes to Ewing sarcoma development by repressing the Na_v1.6 sodium channel and the NF-κB pathway, independently of the fusion oncoprotein

Inmaculada Hernandez-Muñoz¹, Elisabeth Figuerola^{2,*}, Sara Sanchez-Molina^{2,*}, Eva Rodriguez², Ana Isabel Fernández-Mariño^{3,6}, Carlos Pardo-Pastor³, María Isabel Bahamonde³, José M. Fernández-Fernández³, Daniel J. García-Domínguez⁴, Lourdes Hontecillas-Prieto⁴, Cinzia Lavarino², Angel M. Carcaboso², Carmen de Torres², Oscar M. Tirado⁵, Enrique de Alava⁴, Jaume Mora²

¹Fundació Institut Hospital del Mar d'Investigacions Mèdiques (FIMIM), 08003-Barcelona, Spain

²Developmental Tumor Biology Laboratory, Department of Pediatric Hematology and Oncology, Hospital Sant Joan de Déu, 08950-Barcelona, Spain

³Laboratori de Fisiologia Molecular, Departament de Ciències Experimentals i de la Salut, Universitat Pompeu Fabra, 08003-Barcelona, Spain

⁴Department of Pediatric Hematology and Oncology, Instituto de Biomedicina de Sevilla (IBIS), Hospital Universitario Virgen del Rocío/CSIC/Universidad de Sevilla, 41013-Seville, Spain

⁵Sarcoma Research Group, Laboratori d'Oncologia Molecular, Institut d'Investigació Biomèdica de Bellvitge (IDIBELL), L'Hospitalet de Llobregat, 08908-Barcelona, Spain

⁶Present Affiliation: Department of Neuroscience and Biomolecular Chemistry, School of Medicine and Public Health, University of Wisconsin, Madison-53705, USA

*These authors have contributed equally to this work

Correspondence to: Inmaculada Hernandez-Muñoz, **email:** mhernandez@imim.es
Jaume Mora, **email:** jmora@hsjdbcn.es

Keywords: RING1B, Ewing sarcoma, voltage-gated sodium channel, NF-κB, FGFR/SHP2/STAT3

Received: December 10, 2015

Accepted: May 28, 2016

Published: June 15, 2016

ABSTRACT

Ewing sarcoma (ES) is an aggressive tumor defined by *EWSR1* gene fusions that behave as an oncogene. Here we demonstrate that RING1B is highly expressed in primary ES tumors, and its expression is independent of the fusion oncogene. RING1B-depleted ES cells display an expression profile enriched in genes functionally involved in hematological development but RING1B depletion does not induce cellular differentiation. In ES cells, RING1B directly binds the *SCN8A* sodium channel promoter and its depletion results in enhanced Nav1.6 expression and function. The signaling pathway most significantly modulated by RING1B is NF-κB. RING1B depletion results in enhanced p105/p50 expression, which sensitizes ES cells to apoptosis by FGFR/SHP2/STAT3 blockade. Reduced Na_v1.6 function protects ES cells from apoptotic cell death by maintaining low NF-κB levels. Our findings identify RING1B as a trait of the cell-of-origin and provide a potential targetable vulnerability.

INTRODUCTION

Ewing sarcoma (ES) is an aggressive and poorly differentiated tumor, typically arising from bone and soft tissues in children and young adults. It is characterized by reciprocal translocations that result in almost all cases in the fusion of the EWS RNA binding protein 1 (*EWSR1*) to an ETS transcription factor, being *EWSR1-FLII* the most common chimera [1, 2]. ES tumors display a high degree

of genomic stability with very few recurrent mutations besides the pathognomonic fusion, and are among the most genetically normal cancers [3–5]. This strikingly unaltered somatic landscape highlights the role of *EWSR1-FLII* as the unique trigger of the oncogenic transformation in an otherwise yet unidentified cell-of-origin harboring key features that will likely contribute to the eventual development of ES.

Meta-analysis of data coming from *EWSR1-FLII* gain-of-function approaches revealed that the genes up-regulated

by the fusion in heterologous cell systems are more numerous and display more similarities among different experimental models than the genes down-regulated. Since the cell-of-origin of ES remains elusive, gain-of-function models have been carried out expressing the oncogene in a variety of poorly or undifferentiated heterologous cell types. Genome-wide analysis using high-throughput sequencing technologies have identified a plethora of EWSR1-FLI1 direct targets and shown that EWSR1-FLI1 primarily up-regulates gene expression through the interaction with GGAA repeats present in satellite DNA within the genome [6]. In contrast, data obtained by depleting EWSR1-FLI1 in ES cells revealed that many more genes resulted down-regulated by the fusion oncogene than up-regulated, suggesting that gene repression may be more prevalent than transcriptional activation [7]. However, many of these EWSR1-FLI1 repressed targets are divergent and highly dependent on the cellular background [8]. Since EWSR1-FLI1 directly binds to promoters of a small subset of repressed targets [7], the lack of consistency among the different sets of repressed genes is likely due to a variety of both direct and indirect mechanisms used by EWSR1-FLI1 for gene silencing.

EZH2 is a direct EWSR1-FLI1 target that belongs to the Polycomb (PcG) family of epigenetic regulators and blocks endothelial and neuro-ectodermal differentiation of ES cells [9]. PcG proteins form two major families of complexes, the Polycomb-repressive complex (PRC) 1 and 2. PRC2 comprises EED, SUZ12 and EZH2, which catalyzes the K27 trimethylation of histone H3 (H3K27me3). Mammalian PRC1 includes BMI1, MEL18, and RING1B, which catalyzes H2A K119 ubiquitination (ubH2K119) [10, 11]. PRC1 and PRC2 mostly differ in their genomic localization with a small subset of PRC1 co-localizing with H3K27me3. Adding complexity, six major groups of PRC1 subcomplexes with specific developmental functions and mutually exclusive PRC1 subunits have been described, being RING1B the unique common feature [12]. Importantly, it has recently been reported that RING1B catalytic activity results in gene repression, consistent with the classic repressive function of the Polycomb complexes, whereas catalytic-independent association of RING1B with UTX, an H3K27 demethylase, and p300, leads to transcriptional activation [13].

Despite the important role of the epigenetic landscape in ES, studies addressing the PcG contribution to ES tumorigenesis have been restricted to EZH2 and BMI1. Here we investigate the expression and function of RING1B in ES, a protein with unique abilities among the PcG family of epigenetic regulators.

RESULTS

Ewing sarcoma tumors express high levels of RING1B

ES tumors express high EZH2 mRNA levels [9]. To better characterize PcG expression we analyzed EZH2

and RING1B protein expression in ES primary tumors. EZH2 was detected in all the tumor samples, most of them with variable EZH2 expression patterns (Figure 1, right). Particularly poor EZH2 expression was found in largely hemorrhagic tumors, blood clots and tumors infiltrating the adipose tissue (Figure 1, J-N). In contrast, RING1B was highly expressed and uniformly distributed throughout the tumor in most samples, reaching the maximum score (Figure 1, left; Supplementary Figure S1A). Of note, RING1B was expressed in endothelial cells of tumor blood vessels and in the adipose tissue (Figure 1C, 1G), whereas RING1B expression was observed in sparse cells of blood clots (Figure 1F). In these tissues EZH2 expression was low. Importantly, RING1B expression in ES was found to be significantly higher than in other developmental tumors such as rhabdomyosarcoma, synovial sarcoma and Wilms tumor (Supplementary Figure S1B).

Since it has been postulated that neural crest-derived progenitors could be the cell-of-origin [14] and ES tumors display a continuum of different degrees of neural differentiation [15], RING1B expression was also investigated in neural tissues. Moderate RING1B expression was found in cerebellum and peripheral sympathetic ganglia, whereas low or no expression was found in the brain and spinal cord (Supplementary Figure S1C). In addition, RING1B could not be detected in undifferentiated neuroblastic aggregates of the normal fetal adrenal medulla, a derivative of the embryonic neural crest (Supplementary Figure S1C).

Next we analysed the expression of BMI1 and MEL18, two PRC1 proteins. Some specimens displayed low BMI1 and MEL18 levels (Supplementary Figure S2A and S2B), accordingly to reported BMI1 expression in many, but not all, ES primary tumors [16]. In embryonic neural tissues BMI1 expression pattern resembled that of RING1B, with low to moderate expression in most of the embryonic neural tissues (Supplementary Figure S2C).

RING1B expression is independent of EWSR1-FLI1

To test whether RING1B expression was modulated by the oncogene, EWSR1-FLI1 was introduced in 293T and HeLa cells. In both cell lines EZH2 expression was enhanced, as previously reported [9], whereas RING1B levels were not affected (Figure 2A). Conversely, down-regulation of EWSR1-FLI1 in A673 cells resulted in diminished EZH2 levels, but RING1B levels remained unaffected (Figure 2B). Accordingly, endogenous EWSR1-FLI1 binds specifically to a conserved ETS recognition sequence of the EZH2 promoter [17]. In contrast, the genomic region of RING1B was not reported to be an EWSR1-FLI1-direct binding domain [6, 18] nor RING1B was a

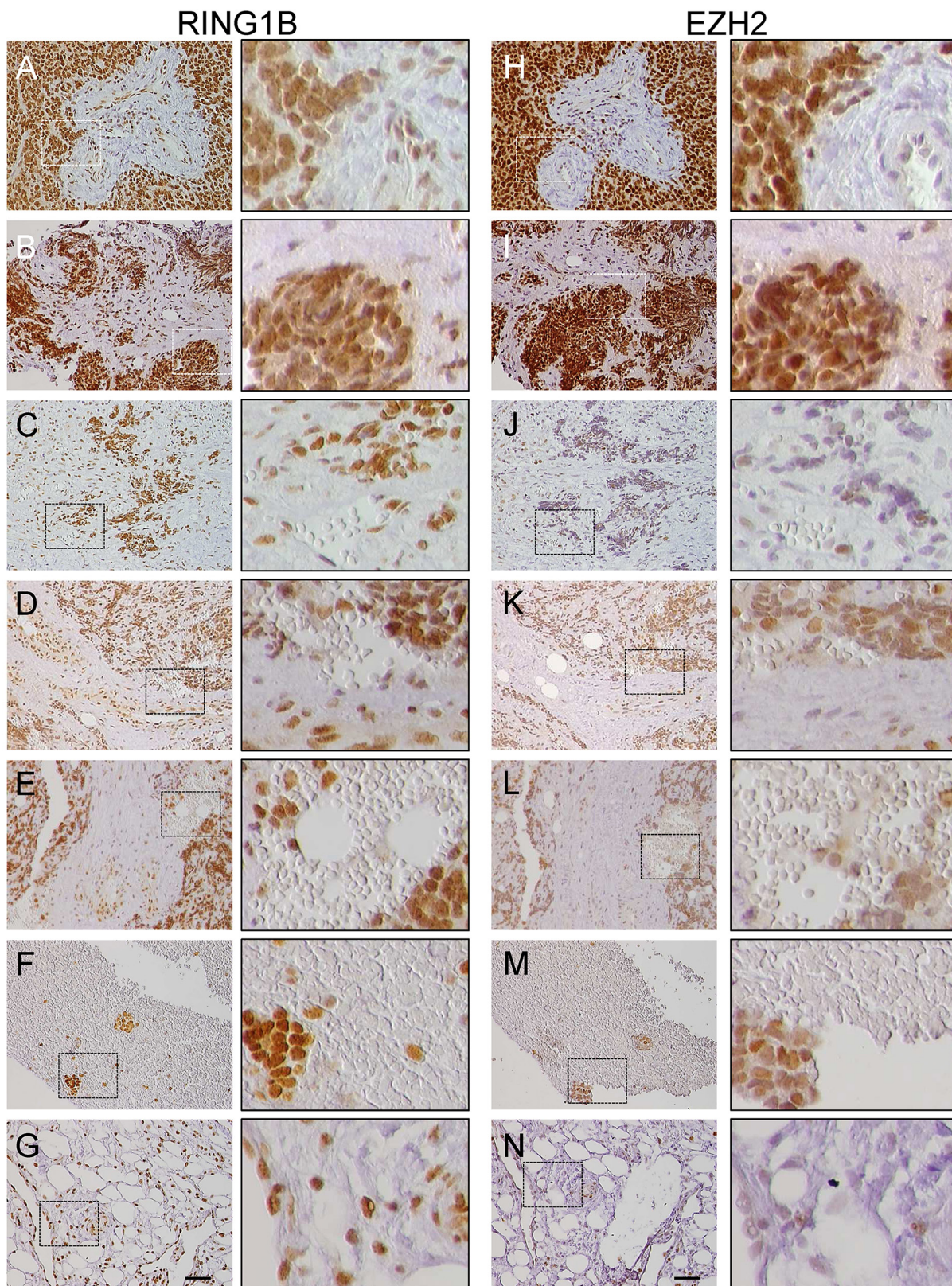


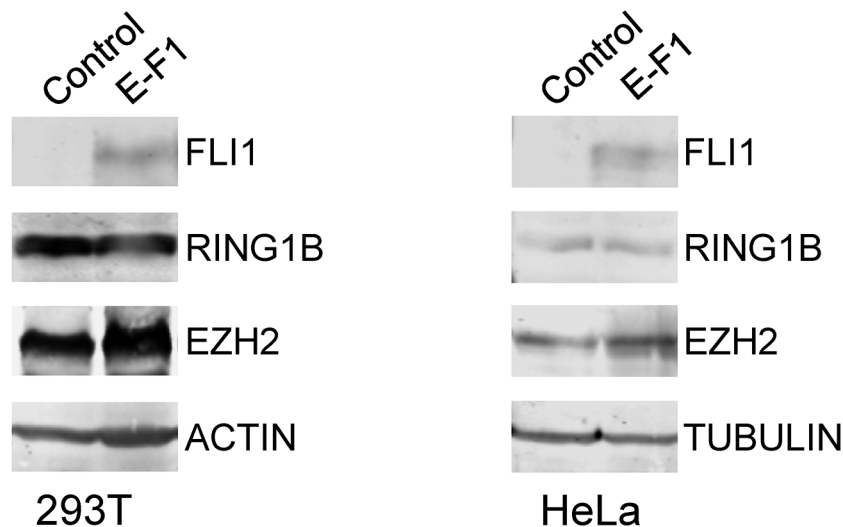
Figure 1: RING1B and EZH2 expression in primary Ewing sarcoma (ES) tumors. Immunohistochemistry analysis of RING1B (A-G) and EZH2 (H-N) expression in serial sections of primary ES tumors. Right columns, higher magnifications of the left panel fields (scale bars 50 μ m). A, B, H, I. samples with intense and homogeneous RING1B and EZH2 staining; C, D, E, J, K, L. hemorrhagic samples with intense RING1B and low EZH2 staining. Blood lakes can be extensively observed in these tumors; F, M. blood clots in an ES sample; G, N. adipose tissue in an ES sample.

differentially expressed gene in EWSR1-FLI1-depleted cells [19, 20]. We suspected that EWSR1-FLI1-independency of RING1B expression might be reflecting the high levels of expression of the cell-of-origin where the oncogenic translocation occur, likely regulating key functions of this cell. Therefore, we decided to study the role of RING1B in ES cells by depleting RING1B protein levels.

Gene expression profile in RING1B-depleted ES cells is unique and enriched in genes functionally involved in hematological development

To identify genes whose expression is regulated by RING1B in ES tumors we analyzed four different ES cell lines stably depleted of RING1B by short hairpin RNA (shRNA) (Figure 3A). Gene expression analysis

A.



B.

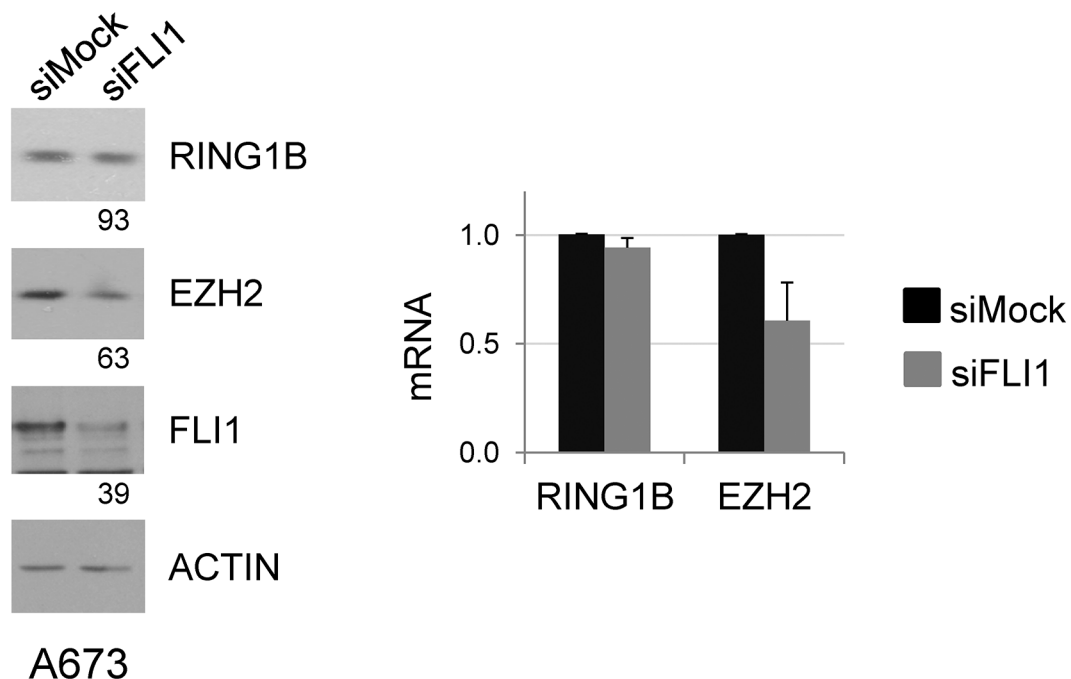


Figure 2: RING1B expression is independent of EWSR1-FLI1. A. EWSR1-FLI1 was ectopically expressed in 293T (left panel) and HeLa (right panel) cells and RING1B and EZH2 levels were determined by western blot. Actin and Tubulin, loading controls. B. A673 cells were transiently transfected with mock or FLI1 short interfering RNA (siRNA) and RING1B and EZH2 levels were determined 48 hours later by western blot (left panel) and qRT-PCR (right panel). Numbers at the bottom represent protein band intensities normalized to Actin and relative to control cells, as described in “Methods”. Graph shows mean \pm SD of three replicate samples from one representative experiment out of three.

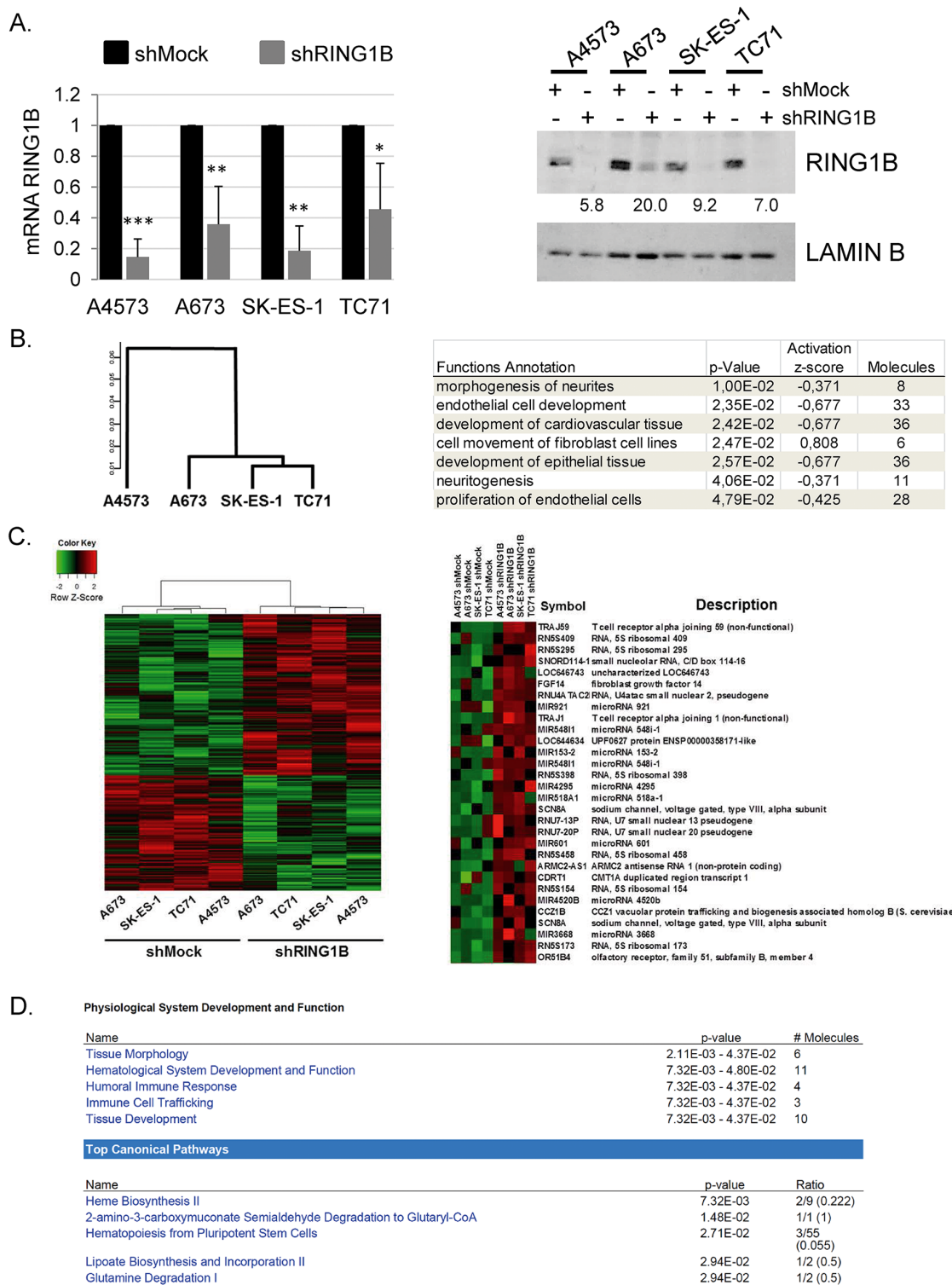


Figure 3: Characterization of the transcriptome in RING1B-depleted ES cells. **A.** Efficiency of stable Ring1B knockdown (short hairpin, sh) in ES cells determined by qRT-PCR (left panel) and western blot (right panel). *, $P < 0.05$; **, $P < 0.01$; ***, $P < 0.005$. Numbers at the bottom, RING1B expression normalized to Lamin B and relative to RING1B levels in each control cell line. **B.** Cluster dendrogram derived from array expression data of the four ES parental cell lines (left panel) and functions of the genes differentially regulated in the A4573 cell line versus A673/SK-ES-1/TC-1 cell lines, identified by the Ingenuity Pathway Analysis (IPA) software (right panel). **C.** Primary heat map of genes differentially expressed between shMock and shRING1B cells. Right panel, heat map depicting the first 30 annotated and up-regulated genes in shRING1B cells. **D.** Top functional annotations enriched among RING1B-regulated genes, identified by IPA software. Array data deposited at the Gene Expression Omnibus (GEO, National Center for Biotechnology Information) with accession number GSE71007.

followed by unsupervised hierarchical clustering of the most variably expressed genes stratified parental cell lines into one main group formed by A673, SK-ES-1 and TC71 and segregated the A4573 cell line (Figure 3B). Of note, A4573 cells also display low BMI1 protein levels [21].

Despite substantial differences in A4573 gene expression profile, linear models for microarrays (LIMMA) analysis was performed using the four cell line data in an attempt to identify common traits of RING1B gene regulation in ES. Logarithmic fold change for each shRING1B/shMock sample pair revealed that RING1B depletion resulted in altered expression of 1430 sequences (Figure 3C). Among them, 523 corresponded to annotated genes, 259 up-regulated (49%) and 264 down-regulated (51%), a ratio that parallels that of RING1B-transcriptionally regulated genes in melanoma [13]. The genes differentially expressed in RING1B-depleted cells were then analyzed at the functional level using the IPA software. This analysis revealed “tissue morphology” and “hematological system development and function” as the top two biological functions altered, while the top canonical pathways identified included “heme biosynthesis” and “haematopoiesis from pluripotent stem cells” (Figure 3D).

To compare RING1B with other PcG proteins, BMI1 was depleted in A673 and TC71 cells (Supplementary Figure S3A). Gene expression analysis revealed that BMI1 or RING1B depletion resulted in 734 and 838 differentially expressed sequences, respectively (Supplementary Figure S3B), 196 overlapping, and among these, 70 were annotated sequences (Supplementary Figure S3C). Most genes, however, were differentially regulated by each PRC1 protein in ES cells.

EZH2 downregulation in ES cells results in the induction of genes important for neural and endothelial differentiation [9]. In contrast, few endothelial and neural genes were identified among the annotated transcripts in RING1B-depleted cells (Figure 4A). Furthermore, RING1B depletion only resulted in enhanced expression of three genes, MS4A3, CDRT1 and TLE4, out of the most significantly EZH2 downregulated genes in ES cells [9] (Figures S4, S5).

All-trans retinoic acid (ATRA)-induced neural stem cell differentiation results in EZH2 down-regulation and decreased binding of EZH2 to ATRA-inducible target genes [22]. Particularly important for ES biology is the differentiation blockade that EZH2 imposes in ES cells, which can undergo neuroectodermal differentiation with butylated hydroxyanisole (BHA) only upon EZH2 depletion [9]. ATRA and BHA treatment of SK-ES-1 cells resulted in reduced EZH2, but not RING1B, mRNA levels (Figure 4B). Furthermore, neither ATRA nor BHA were able to induce differentiation in shRING1B cells since mRNA levels of neural and endothelial differentiation genes remained similar to those of the untreated cells (Figure 4C).

RING1B regulates the Na_v1.6 sodium channel in Ewing sarcoma cells

FGF14 and SCN8A were among the top 30-upregulated annotated sequences upon RING1B depletion (Figure 3C), and these increases were validated by qRT-PCR in RING1B-depleted cells (Figures 5A, S6A). *SCN8A* encodes the α subunit of the voltage-gated sodium channel type VIII, or Na_v1.6. This protein forms a sodium-selective channel essential for rapid membrane depolarization in response to voltage differences in excitable neurons. FGF14 is a member of the intracellular fibroblast growth factor subfamily (iFGF) that co-localizes and interacts with the Na_v channel α subunits, being Na_v1.6 the most sensitive to FGF14 modulation [23]. While RING1B was not detected at the FGF14 promoter (data not shown), it was found to bind to the promoter region of the *SCN8A* gene in ES cells (Figure 5B). RING1B depletion using an independent shRNA construct [11] confirmed that *SCN8A* is repressed by RING1B in ES cells (Supplementary Figure S6B). *SCN8A* released expression in RING1B-depleted cells resulted in enhanced Na_v1.6 protein levels (Figure 5C). In contrast, RING1B depletion in 293T did not affect Na_v1.6 levels (Figure 5C) while in neuroblastoma SK-N-SH cells caused subtle increases in *SCN8A* mRNA levels (Figures S6C), suggesting that RING1B regulation of the Na_v1.6 channel is specific of ES cells.

Next we investigated Na_v1.6 channel regulation by other PcG proteins. BMI1 depletion resulted in *SCN8A* down-regulation while EZH2 depletion lead to minor changes in *SCN8A* mRNA levels (Supplementary Figure S7). Furthermore, treatment with the histone methylation inhibitor DZNep did not affect *SCN8A* mRNA levels (Supplementary Figure S7D). All these data suggest that Na_v1.6 channel repression in ES is specifically set by RING1B.

To check the functional impact of the enhanced expression of Na_v1.6 upon RING1B depletion we used the voltage-clamp technique in the whole-cell configuration to record voltage-gated sodium currents. In response to depolarizing pulses, significant fast-activating and fast-inactivating inward sodium currents, with a persistent component (consistent with Na_v1.6 electrophysiological properties [24, 25]), were only recorded in shRING1B cells but not in shMock control cells (Figure 5D). Since Na_v1.6 knockout in dorsal-root ganglion cells results in migration towards the ventral region and acquisition of a parasympathetic phenotype [26] we investigated the migratory abilities of ES cells. A4573 and A673 control cells displayed migratory abilities that were attenuated in RING1B depleted cells (Figure 5E). Since RING1B depletion affects the expression of very few neural genes and did not alleviate ES cells from their neural differentiation blockade, this result suggests that targeted Na_v1.6

repression might be of particular relevance for ES biology.

RING1B modulates the NF-κB pathway in Ewing sarcoma cells

To identify molecular pathways affected by RING1B-modulated targets we conducted IPA. On the basis of the four RING1B-depleted cell line signature,

the IPA analysis revealed NF-κB as the most significantly altered node (Figure 6A). To explore this pathway we performed western blot analyses of the five members of the NF-κB transcription factor family: NF-κB1 (p50 and its precursor p105), NF-κB2 (p52 and its precursor p100), c-Rel, RelA/p65 and RelB. Levels of p105 and p50 were enhanced to variable degrees in shRING1B cells when compared to their corresponding shMock controls (Figure 6B). RING1B depletion using an independent

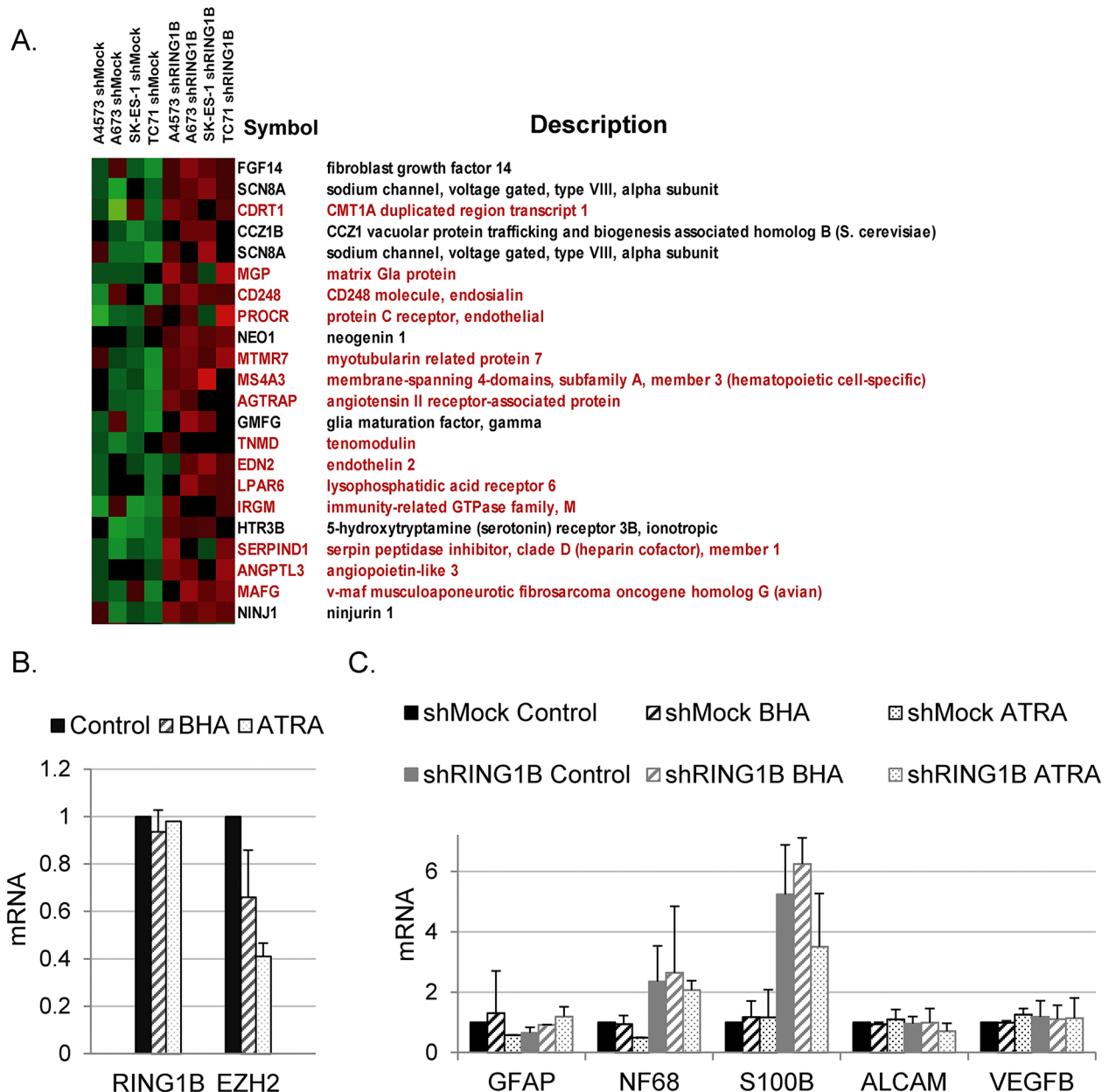


Figure 4: RING1B depletion does not result in global alterations of developmental transcription programs in ES cells. **A.** Heat map showing endothelial (red) and neural (black) genes up-regulated in RING1B-depleted cells, identified by manual curation of the microarray annotated sequences. **B.** RING1B and EZH2 mRNA levels determined by qRT-PCR in SK-ES-1 cells treated with differentiating agent butylated hydroxyanisole (BHA) and all trans-retinoic acid (ATRA). **C.** SK-ES-1 cells, either shMock or shRING1B, were treated with BHA or ATRA and mRNA levels of different neural or endothelial genes were analyzed by qRT-PCR. B and C. graphs show mean ± SD from two independent experiments performed with three replicate samples.

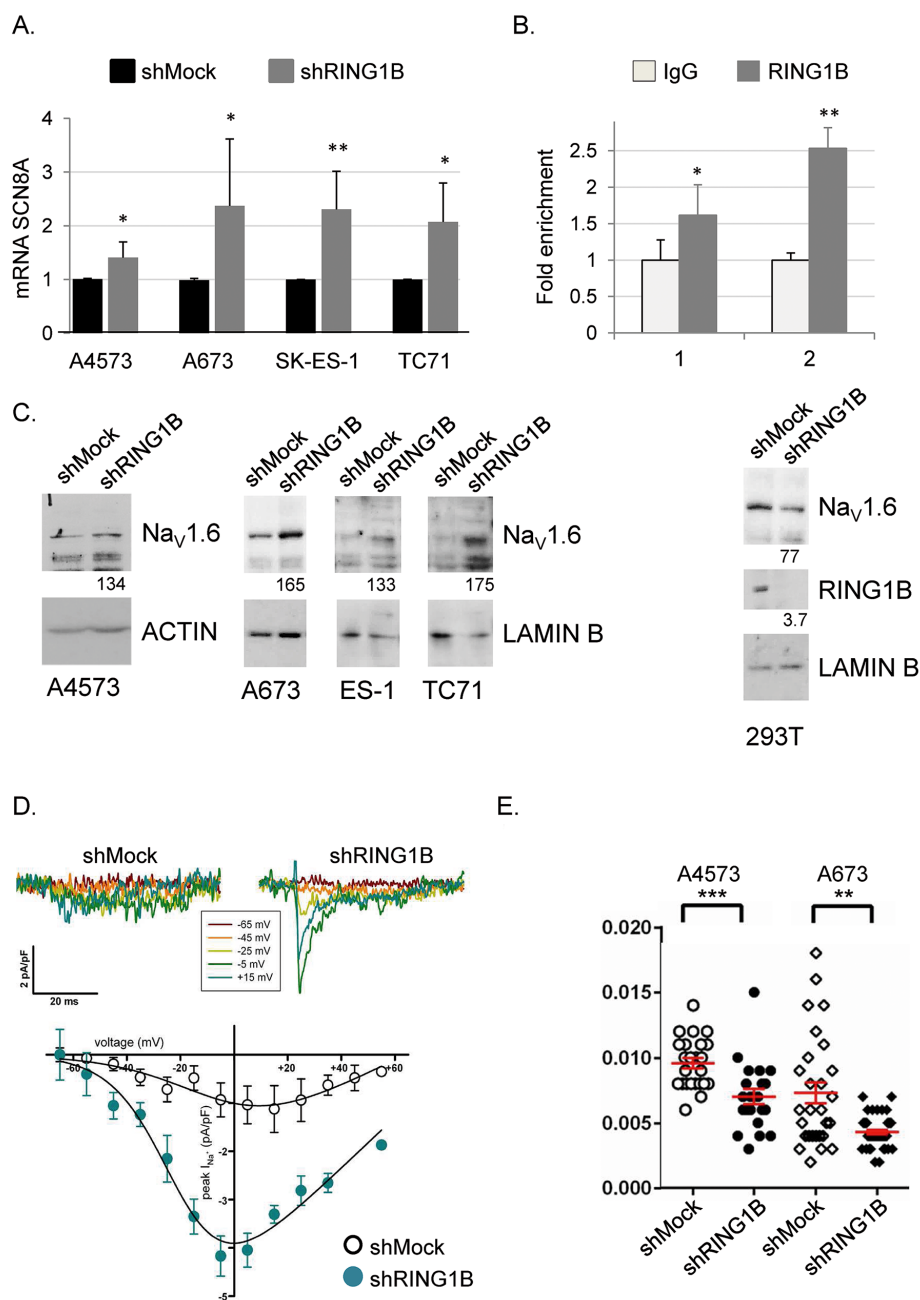
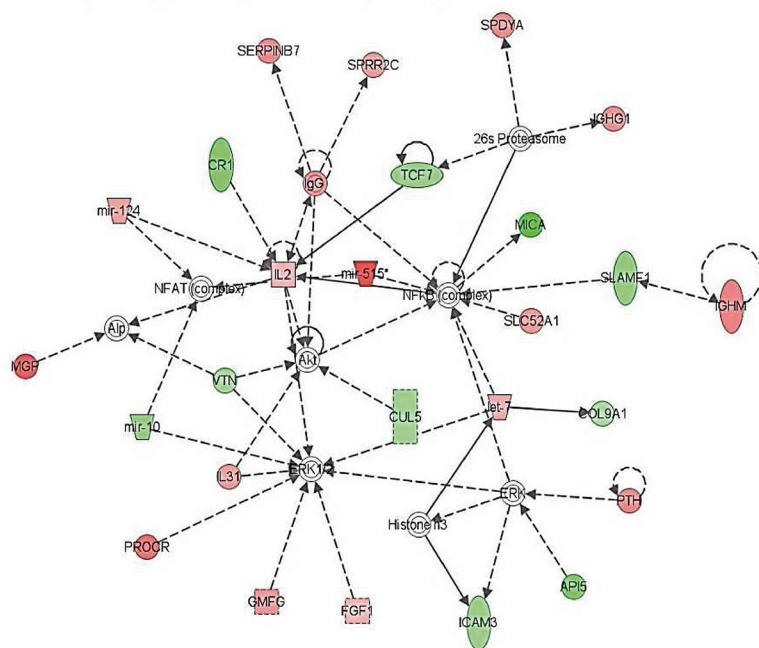
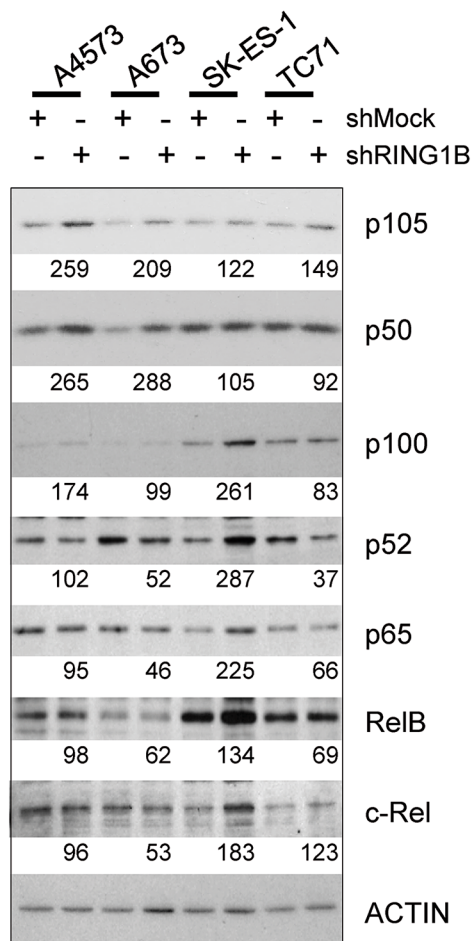


Figure 5: RING1B represses the NaV1.6 channel in ES cells. **A.** SCN8A mRNA levels in RING1B-depleted cells determined by qRT-PCR and referred to shMock control mRNA levels. *, P < 0.05; **, P < 0.01. **B.** Relative enrichment of RING1B occupancy at SCN8A promoter, measured by ChIP-qPCR. Graph displays percentage of RING1B recruitment to two different SCN8A promoter amplicons, referred to enrichment from the IgG control, set as 1. Data express mean ± SD of three independent experiments. *, P < 0.05; **, P < 0.01. **C.** Na_v1.6 protein levels in cytoplasmic (A4573) and total (A673, SK-ES-1, TC-71, 293T) extracts from control or RING1B-depleted cells, analyzed by immunoblot. Numbers at the bottom, band intensities normalized to Actin or Lamin B and relative to control cells. **D.** Representative current traces obtained from shMock and shRING1B SK-ES-1 cells clamped at -90 mV and pulsed for 40 ms to the indicated depolarizing voltage (top) and average current density-voltage (I-V) relationships for shMock (open circles, n = 5) and shRING1B (filled cyan circles, n = 5) cells (bottom). Fast-activating inward currents with both transient and persistent components, consistent with Na_v1.6 currents, were only observed in shRING1B SK-ES-1 cells (peak current was 4.2 ± 0.4 pA/pF) and the corresponding V_{1/2} act, kact and Vrev values after fitting the I-V curve to a Boltzmann equation (see Methods for further details) were (in mV): -21 ± 4.1 mV (as reported for Na_v1.6 channels heterologous expression in the ND7/23 neuronal cells, either in the absence or presence of FGF14 (54;61)), 10.8 ± 2.1 and 84.5 ± 16.3 , respectively. **E.** Cell migration speed measurements (in micron/sec) during wound healing from shMock (open) and shRING1B (black filled) A4573 and A673 cell lines (obtained in three different experiments). Symbols represent individual cells. Red bars depict mean ± SEM speed. Suppressing RING1B expression, which correlates with increased SCN8A expression, decreased cell speed in A4573 and A673 cells. **, P < 0.01; ***, P < 0.001.

A.



B.



C.

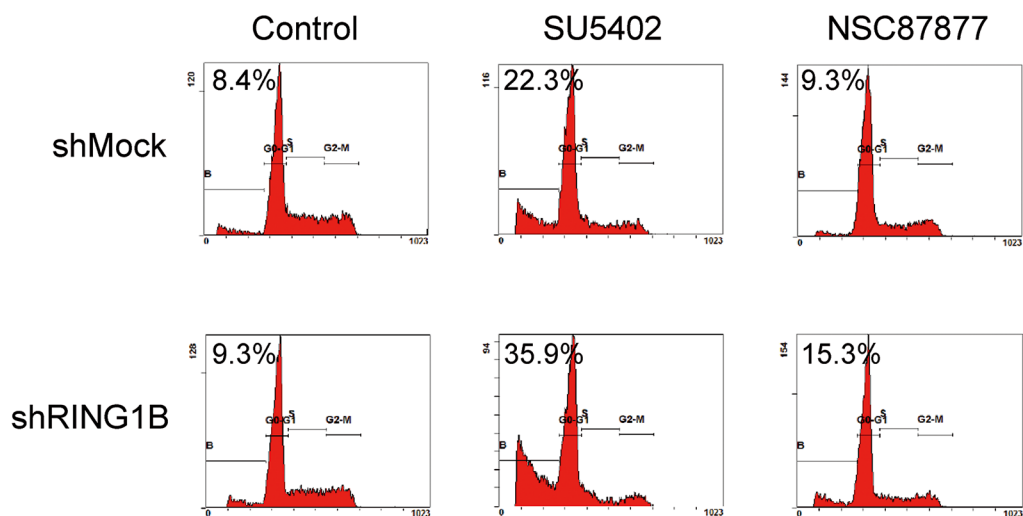


Figure 6: RING1B represses NF- κ B in ES cells. **A.** Top-scoring multigene network associated by the IPA software to microarray expression data in RING1B-depleted cells. Overexpressed genes, red; downregulated genes, green. **B.** Levels of NF- κ B proteins, detected by immunoblot performed using total extracts of shMock and shRING1B cells. Numbers at the bottom, band intensities normalized to Actin and relative to their own control cells. **C.** Flow cytometry analysis of A673 cells treated with 25 μ M SU5402 or 50 μ M NSC87877 for 24h. Percentage of cells in the sub-G1 region is indicated. DNA histograms of 10,000 propidium iodide stained cells.

shRING1B also resulted in consistently enhanced p50 levels (Supplementary Figure S8A). RING1B-depletion in non-ES cells like 293T and SK-N-AS (neuroblastoma) displayed inconsistent changes in NF- κ B1 levels (Supplementary Figure S8C).

Since the NF- κ B pathway is a regulator of stress response, next we checked the sensitivity of ES cells to challenging conditions. A673 cells were subjected to a panel of chemical inhibitors and cell viability was tested by flow cytometry using propidium iodide staining. Two drugs induced significant apoptotic cell death: SU5402 and NSC87877. Whereas SU5402 irreversibly blocks FGF and VEGF tyrosine kinase receptors [27], NSC87877 specifically inhibits SHP2 [28], a tyrosine phosphatase that participates in the regulation of FGFR signalling [29]. Interestingly, RING1B-depleted cells treated with these inhibitors showed enhanced sub-G1 peaks when compared to shMock cells (Figure 6C). To better characterize this effect, the four ES cell lines, either shMock or shRING1B, were treated with the two inhibitors. NF- κ B1 levels in shRING1B cells remained elevated compared to their own shMock controls regardless of the inhibitor treatment (Supplementary Figure S8B). SU5402 and NSC87877 treatments resulted in enhanced cleaved PARP1 levels in shRING1B cells when compared to controls (Figure 7A), indicating that RING1B depletion sensitizes ES cells to the apoptosis induced by the FGFR-SHP2 blockade. In contrast, RING1B depletion in 293T and SK-N-AS cells did not affect cleaved PARP levels (Figure 7B). I κ B kinase (IKK) α/β inhibition with BMS-345541 attenuated SU5402-induced PARP1 cleavage in A673 shRING1B cells, further suggesting that NF- κ B is pivotal for RING1B-mediated sensitivity to apoptosis in ES cells (Figure 7C).

Activation of FGFRs results in the stimulation of several signaling pathways including STAT3. Therefore, we investigated the sensitivity of ES cells to the STAT3 inhibitor S31-201. As shown in Figure 7D, ES cells viability was affected at significantly lower concentrations of S31-201 than 293T cells. RING1B depletion further sensitized ES cells to S31-201, as shown by the appearance of cleaved PARP1 at lower inhibitory concentrations compared to control cells (Figure 7E).

Increases in intracellular sodium through voltage sensitive sodium channels can contribute to apoptotic cell death [30]. Therefore we asked whether the enhanced Na_v1.6 functionality in RING1B depleted cells increased the sensitivity of ES cells to apoptosis by selective blocking of the voltage-sensitive sodium channel with Tetrodotoxin (TTX). A673 shRING1B cells treated with SU5402, NSC87877 or S31-201 and cultured in the presence of TTX showed decreases in p105 and p50 levels and lower cleaved PARP levels than cells cultured in the absence of TTX, suggesting that RING1B repression of Na_v1.6 also contributes to protect ES cells from apoptotic cell death by maintaining low NF- κ B levels (Figure 7F).

DISCUSSION

Recent next-generation sequencing studies have revealed the simplicity of the ES genome [1, 3-5] highlighting the critical importance of the *EWSR1-ETS* fusion event. The mechanism by which *EWSR1-FLI1* contributes to tumorigenesis is complex since the fusion oncogene affects the cell in many different ways. The best known function of the EWSR1-FLI1 protein is that of an aberrant transcription factor. However, other EWSR1-FLI1 properties including RNA binding, RNA splicing and protein-protein interactions are increasingly being recognized as fundamental to understand the plethora of effects induced by the fusion oncogene. Equally important has been the recognition of the critical role of the cellular context for EWSR1-FLI1 activity. In normal murine and human fibroblasts, *EWSR1-FLI1* by itself does not transform cells; instead, it results in cell cycle arrest [31]. Related to this is the fact that it has been very difficult to establish an appropriate animal model by introduction of *EWSR1-FLI1* chimeras, suggesting that *EWSR1-FLI1* is not sufficient to define the origin of ES. Finding universal features for a cell-of-origin to tolerate *EWSR1-ETS* chimeras would be extremely helpful to understand ES tumorigenesis. Here, we show that RING1B is highly and universally expressed in primary ES tumors. We also show that RING1B expression is not a direct target of the fusion oncogene and that RING1B levels are not affected by chemically induced differentiation of ES cells. Furthermore, we demonstrate that RING1B regulates, independently of the fusion oncogene, critical pathways that may reflect the biology underlying the cell of origin.

Chromatin repressive complexes like the PcG protein complexes PRC1 and PRC2 are essential mediators of stemness and critical contributors to cancer pathogenesis by suppressing the expression of tumor-suppressor genes and developmental regulators in a context-dependent, cell-type-specific manner [32]. Our data show an intense and universal expression of RING1B in ES primary tumors, in contrast with other PRC proteins which are selectively expressed in some but not all ES tumoral cells. Indeed BMI1 expression is variable among both primary tumors and cell lines in our experience and in previously published studies [21] and EZH2 expression is heterogeneous in most of ES primary tumors. A particularly low EZH2 expression was found in hemorrhagic areas and blood lakes and in tumors infiltrating the adipose tissue. Blood lakes are a striking feature of ES first recognized by James Ewing, which led him to describe the tumor as an endothelioma [33]. Van der Schaft and colleagues described an abundant presence of blood lakes and vascular-like tube formations, suggesting a contribution of the blood lakes to circulation recalling vasculogenic mimicry [34], as had previously been described in melanoma [35]. The lower expression of EZH2 in the blood lakes in our study is consistent with the

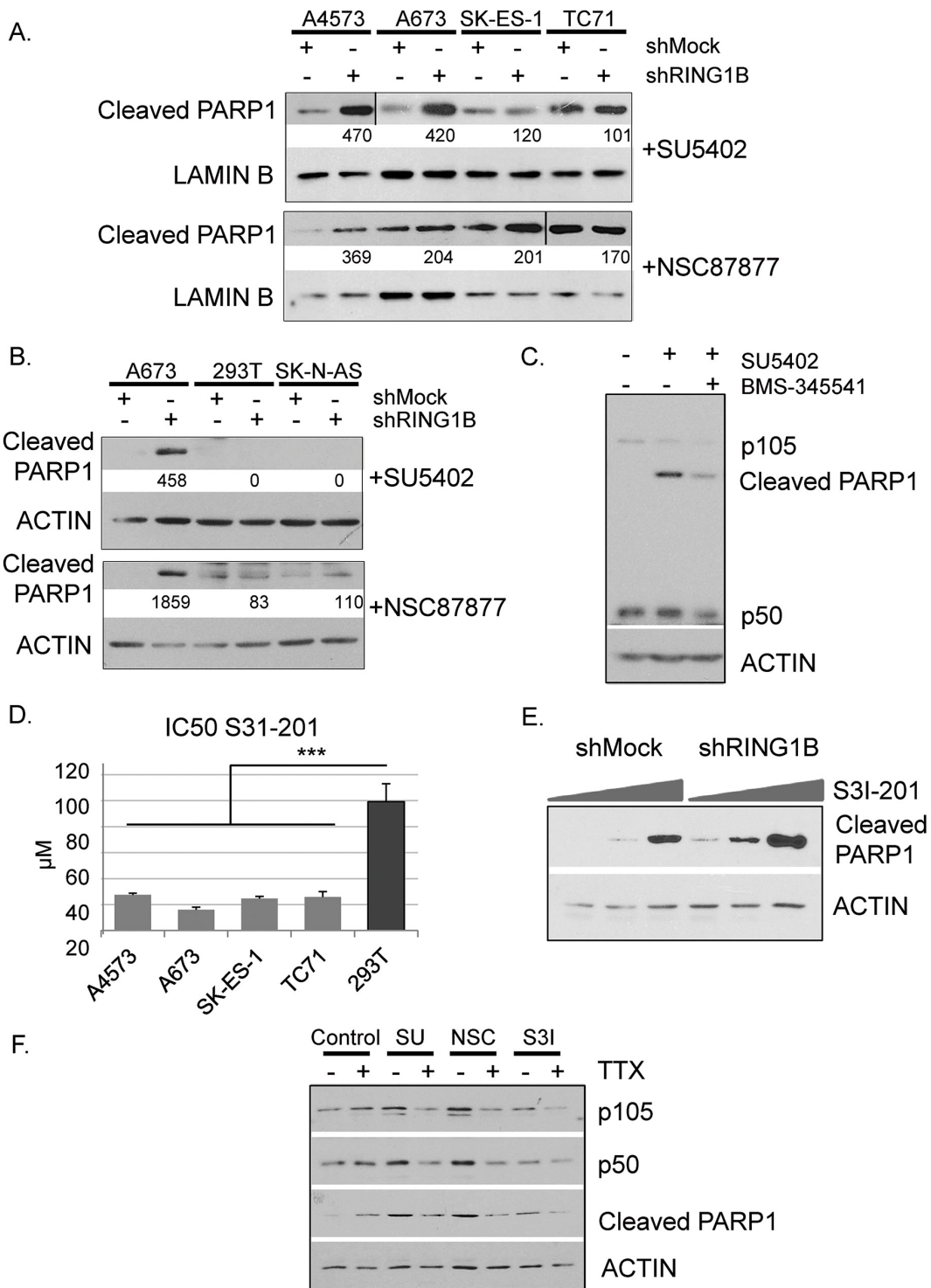


Figure 7: RING1B down-regulation sensitizes ES cells to undergo NF- κ B-mediated apoptosis induced by FGFR signaling blockade. **A.** Immunoblot detection of cleaved PARP1 in shMock and shRING1B cells treated with 25 μ M SU5402 or 50 μ M NSC87877 for 24h. **B.** Immunoblot detection of cleaved PARP1 in 293T embryonic and SK-N-AS neuroblastoma cells, treated as above. Numbers at the bottom, band intensities normalized to Actin or Lamin B and relative to their own control cells. **C.** Immunoblot detection of NF- κ B1 (p105 and processed form p50) and cleaved PARP1 in A673 shRING1B cells after 24h with or without 25 μ M SU5402 and the inhibitor of the I κ B kinase (IKK) α/β BMS-345541 at 300nM. **D.** Half maximal inhibitory concentration (IC50) values for S31-201 in ES and 293T cells, measured after 72h treatment and expressed as mean \pm SD (n=3). ANOVA-Bonferroni post-hoc test, *** <0.001. **E.** Cleaved PARP1 in shMock and shRING1B A673 cells, after 24h treatment with the STAT3 inhibitor S31-201 at 25 μ M, 50 μ M and 100 μ M. **F.** Levels of the NF- κ B subunits p105 and p50, and cleaved PARP1 in shRING1B A673 cells, after 24h treatment with 25 μ M SU5402, 50 μ M NSC87877 or S3I-201 at 50 μ M in the absence or the presence of 1 μ M Tetrodotoxin (TTX).

inhibitory function of EZH2 on endothelial differentiation [9]. In these cells RING1B retains a relatively high level of expression suggesting that RING1B could be important in an endothelial cell context. In this regard, it is notable that NF- κ B has been shown to be crucial for endothelial cell fate determination and that NF- κ B activation results in apoptosis in endothelial cells [36]. Similarly, we here report that, in shRING1B ES cells, enhanced NF- κ B levels are detrimental and sensitize ES cells to apoptosis. Our results also help to explain previous studies reporting very low NF- κ B activity in ES [37–39] and suggest that NF- κ B is to be repressed in the ES cell-of-origin because elevated NF- κ B levels in such cells result in apoptosis. According to our data, the ES cell-of-origin displays traits of endothelial-precursor cell biology.

FGF receptors (FGFRs) include a family of high- and low-affinity bFGF receptors. bFGF, a ubiquitously expressed growth factor that affects a broad spectrum of developmentally regulated cellular responses, induces cell death in ES [40]. Since bFGF has a critical role in the commitment of primitive neural cells toward a neuronal phenotype, the induction of apoptosis in ES was thought to be consistent with the hypothesis that Ewing tumors arise in a primitive neural stem cell. However, the magnitude of bFGF-induced cell death was heterogeneous suggesting that ES can arise from primitive cells at various stages and that the expression of different growth factors and hormones by Ewing tumors may modulate the effect of bFGF [41]. Our results suggest that RING1B regulates the apoptotic response of FGFR activation in ES cells and thus it could be the modulator element proposed in previous publications between extracellular signaling (hormones and growth factors) and cell type response. More recently, the FGF/FGFR signaling has been found to play a vital role in the development and maintenance of bone growth at growth plates [42]. Since we provide evidence of an active FGF/SHP2/STAT3 pathway in the potential Ewing cell-of-origin, a putative relationship with normal bone growth and development deserves further investigation.

STAT3 is known to drive pathways regulating normal cell growth, which result in tumorigenesis when deregulated [43]. Reportedly, 50% of ES primary tumors express activated/phosphorylated STAT3 [44, 45] and germline mutations of Protein tyrosine phosphatase delta (PTPRD, a STAT3 phosphatase) have recently been described in three ES patients [46]. Aberrant activation of STAT3 signaling participates in the initiation, development and progression of human cancers via induction of STAT3 downstream genes that encode antiapoptotic proteins, cell cycle regulators and angiogenic factors such as Bcl-2, Cyclin D1 and VEGF [47]. Also, increased macrophage infiltration and tumor microvascular density have been noted in tumors from ES patients with poor prognoses and tumor associated macrophages are known to express high concentrations of cytokines that lead to aberrant activation of the JAK/STAT3 pathway. In addition, EWSR1-FLI1

inhibition in ES cells resulted in the secretion of soluble factors, such as IL6, that activate STAT3 in bystander (non-targeted) ES cells, protecting them against apoptosis [48]. Since NF- κ B modulates the expression of a variety of cytokines, release of NF- κ B inhibition upon RING1B knockdown could result in a feed forward loop of STAT3 activation and cytokine production. This adaptive response suggested that combination therapy with STAT3 inhibitors may increase the efficacy of targeted therapeutics in ES. Reports on JAK/STAT3 inhibitors have shown *in vitro* and *in vivo* activity against ES. For instance, Thiele *et al.* have shown the antitumoral activity of the JAK1/2 inhibitor AZD1480 blocking endogenous constitutive and cytokine-induced activation of STAT3 *in vitro* and suppressing the growth of ES xenografts *in vivo* [49]. Our results showing higher sensitivity to STAT3 inhibition in RING1B-depleted cells suggest that combined inhibition of RING1B and STAT3 could generate enhanced antitumor effects against ES (proposed model in Figure 8). Inhibition of STAT3 activity is well-known to enhance chemosensitivity of multiple tumor types to a number of different cytotoxic agents or other targeted agents; therefore multiple combinations of target inhibition of key pathways for ES like RING1B and STAT3 together with conventional chemotherapy could represent a novel approach for ES patients.

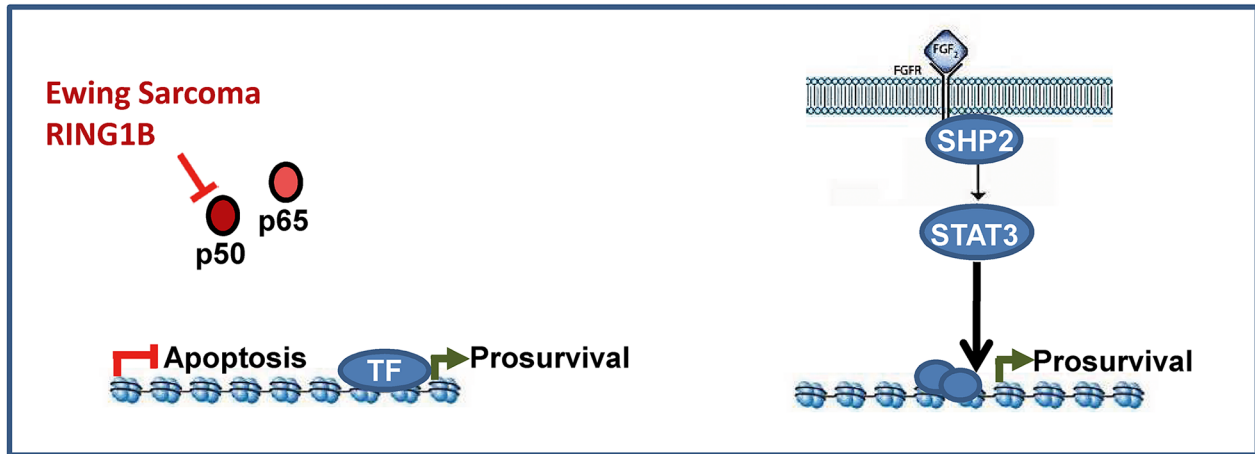
The role of PcG increasing the chances for the cancer cell to survive in hostile microenvironments has recently been shown in ES and other tumors by Lawlor *et al.* [50]. They described KCNA5 repression by BMI1, and the impairment in the execution of hypoxia-induced apoptotic cell death. In this study we show that Na_v1.6 regulation in ES is specific to RING1B, not being shared with other PcG proteins. RING1B represses the expression and function of this sodium channel, normally expressed in central neurons, dorsal root ganglia, peripheral neurons, heart, and glial cells. The selectivity of this regulation by RING1B is striking because many other neural genes are actively induced by the *EWSR1-ETS* fusion, globally resulting in a neural-like phenotype of the ES cell. Together with the well-known migration blockade caused by *EWSR1-FLI1* in the chicken model [51] and our results would suggest co-regulation of the cellular migratory properties of ES cells by RING1B and the fusion oncogene.

The origin of ES has been an enigma since the first case was reported in 1921 [33]. Primitive neural crest cells, hematopoietic cells, and muscle cells as well as mesenchymal stem cells (MSC) have been considered possible cells of origin [52, 53]. Histologically, ES has a certain resemblance to primitive neuroectodermal cells [54]. Early neural markers are present in some tumors and ultrastructural features of neural cells can also be observed in some cases [15, 55, 56]. Furthermore, ES cells can be induced to differentiate in the laboratory towards the neural lineage [57]. Conversely, introduction of *EWSR1-FLI1* into neuroblastoma cells has been shown to make the cells acquire

characteristics of ES [58]. *EWSR1-FLI1* has been shown to induce neuroectodermal differentiation and up-regulate a number of genes associated with early neural differentiation [59]. Altogether, these findings raise the possibility that the neuroectodermal characteristics of the ES cell might be a direct result of *EWSR1-FLI1* expression and not necessarily reflect a feature of the cell-of-origin.

An alternative hypothesis is that ES derives from a MSC. Although cranial bones develop from mesenchymal condensation of neuroectoderm [52], the long bones of the limbs originate from mesoderm [60] and there may not normally be primitive neuroectodermal cells in that bone. However, bone marrow mesenchymal cells can exhibit some characteristics of neuroectodermal cells [61, 62].

A.



B.

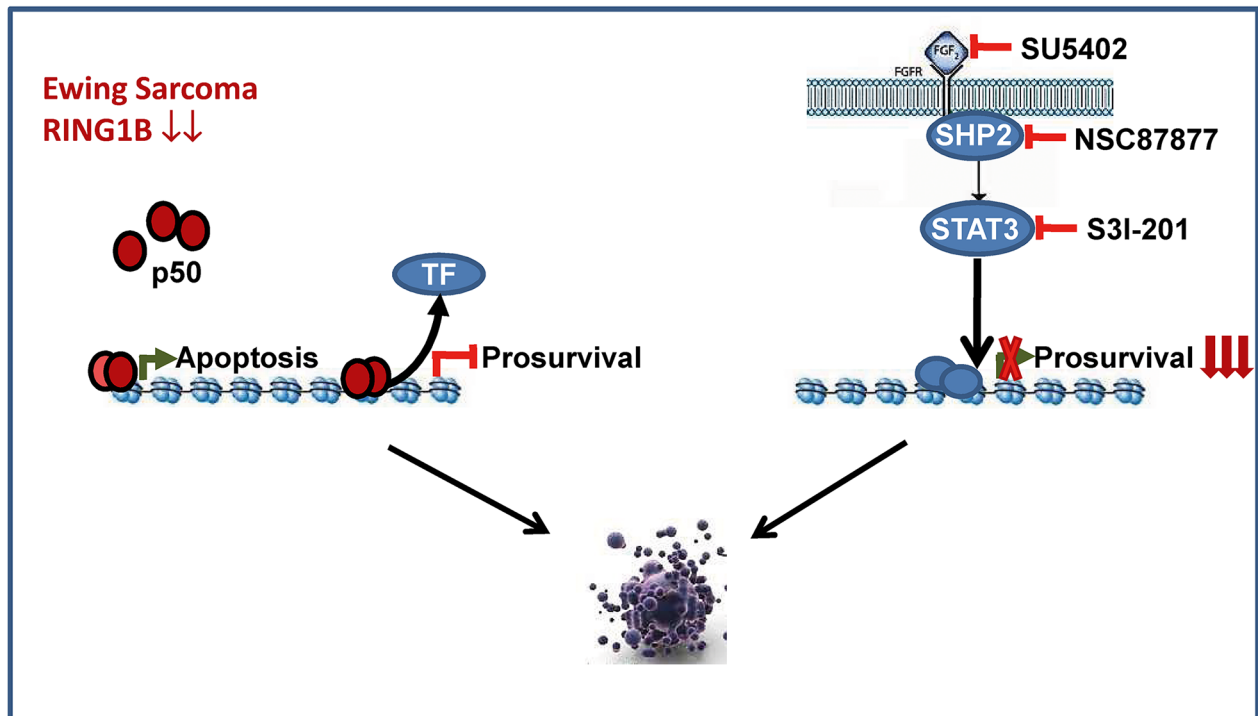


Figure 8: Proposed model for RING1B-dependent antiapoptotic function in ES. A. According to our results we propose an endothelial lineage of the ES cell-of-origin where bFGF/VEGF are specially active and, upon binding to their receptors, activate a signaling cascade that transmits a nuclear signal prompting target genes to activate cell growth. As reporter for an endothelial progenitor cell (EPC) characteristic biology, proapoptotic genes remain inactive in cells with low NF- κ B levels tightly controlled by RING1B in ES cells. B. Similar to EPC when treated with antiangiogenic factors, RING1B depletion in ES cells results in NF- κ B activation, which binds to proapoptotic gene promoters and/or displaces transcription factors from prosurvival gene promoters. In this situation ES cells are highly sensitive to FGF/SHP2/STAT3 blockade (adapted from [36]).

These cells can also be induced *in vitro* to differentiate towards the neural lineage [63, 64]. The term MSC usually implies a cell that has the capacity to differentiate towards various mesodermal lineages. Indeed, EWSR1-FLI1 knockdown revealed that ES cells have some capacity for *in vitro* differentiation towards chondroblastic, osteoblastic and adipocytic lineages [53]. Furthermore EWSR1-FLI1 expression in mesenchymal cells resulted in development of ES tumors [65, 66] and *EWSR1-FLI1* introduction into a population of cells enriched for osteochondrogenic progenitors derived from the embryonic superficial zone of murine long bones revealed a subpopulation of precursor cells that further enhanced EWSR1-ETS-dependent tumor induction [67]. It is yet unclear whether there is a special subfraction of precursor cells that includes the cell of origin of ES, although Stamenkovic and colleagues have reported that primary ES tumors harbor a subpopulation of cells that express CD133 constituting 3-15% of tumor cells that display the plasticity, clonogenicity and tumor-initiating capacity of tumor stem cells [68].

Murine studies have shown that the target cells of *EWSR1-ETS* might be cells of a narrow lineage of MSC and/or of a limited differentiation stage in support of a mesenchymal origin of ES. However, the simple knockdown of EWSR1-FLI1 in tumor cells does not cause them to revert to a normal mesenchymal cell. Constitutive expression of EWSR1-FLI1 protein in embryonic stem cells causes cell death [69], and mice with expression of *EWSR1-FLI1* in the whole body have an embryonic lethal phenotype [70]. Target expression to bone marrow progenitor cells surprisingly produced leukemias [70]. *EWSR1-FLI1* conditional expression in the mesoderm-derived tissues of the limbs resulted in limb shortening, muscle atrophy, osseous dysplasia and other developmental abnormalities [71]. However, sarcomas did not spontaneously form unless the p53 gene was simultaneously mutated [71].

After all, it would seem that the “cell-of-origin” concept for ES may turn out as too simplistic. *EWSR1-FLI1* may be fully transforming only cells that possess the right conditions, which are likely very limited during development. Such a narrow window of target cell emergence would explain the difficulty of inducing tumors in *in vivo* models. We suggest that RING1B is one defining epigenetic precondition for the oncogenic fusion to occur and, at least for some cases, reflects the cellular background of a hemato-endothelial precursor cell as the cell of origin.

MATERIALS AND METHODS

Study approval

A written informed consent was received from all patients prior to inclusion of their samples in the Hospital Sant Joan de Déu (HSJD) tumor biobank. Sixteen primary

ES specimens were used in the study. Procedures were approved by the Ethical Committee for Clinical Research at HSJD.

Immunohistochemistry

Immunohistochemical analyses were performed following standard techniques [72]. RING1B and BMI1 antibodies were purchased from Millipore and EZH2 and MEL18 antibodies from Cell Signaling. Immunohistochemical staining was scored for staining intensity and proportion of stained cells by two independent investigators. A semiquantitative histoscore (0×% negative cells + 1×% weakly stained cells + 2×% moderately stained cells + 3×% strongly stained cells) was generated for statistical analysis. This histoscore thus has a range of possible scores between 0 and 300. Statistical analysis was performed with the Wilcoxon signed rank test.

Gene expression analysis

Microarray analysis, amplification, labeling and hybridizations were performed according to protocols from Ambion WT Expression Kit (Ambion), labeled using the WT Terminal Labeling Kit (Affymetrix), and then hybridized to GeneChip Human Gene 2.0 ST Array (Affymetrix).

Electrophysiology

Whole-cell voltage-clamp recordings from shMock and shRING1B ES1 cells were obtained using a D-6100 Darmstadt amplifier (List Medical) filtered at 1 kHz and corrected for leak and capacitive currents using the leak subtraction procedure (P/8). Data are expressed as mean ± SEM. For the generation of current-voltage (I-V) curves, peak inward Na⁺ currents were measured from cells clamped at -90 mV and pulsed for 40 ms from -65 mV to +55 mV in 10 mV steps. Single I-V curves at each experimental condition were averaged to obtain the shown I-V curves.

Flow cytometry

Sub-G1 population staining was performed as previously reported [73] and the analysis was performed by FACScan (Coulter).

Cell viability assay

Cells were seeded at 3000 per well in 96-well culture plates. S3I-201 (STAT3 inhibitor) was added to complete growth medium at concentrations ranging from 1 to 200 μM, respectively. After 72 h, cells were subjected to the ATPlite assay (PerkinElmer, Waltham, MA, USA) and inhibitory concentrations were calculated.

Statistics

Each experiment was performed in triplicate at least three times unless otherwise indicated. Statistical analysis was performed with Student's t-test. $P < 0.05$ was considered significant.

Extended methods on cell culture, protein and mRNA analysis, gene expression arrays and electrophysiology are available as *Supplemental Information*.

ACKNOWLEDGMENTS

We thank L. Nonell, S. Mojal (FIMIM) and S. Pérez-Jaume (FSJDD) for their technical support.

GRANT SUPPORT

IHM is a Miguel Servet investigator (Instituto de Salud Carlos III, ISCIII). This work was supported by the Xarxa de Bancs de Tumors de Catalunya sponsored by Pla Director d'Oncologia de Catalunya and by grants from ISCIII-FEDER (PS09/00973; RIC RD12/0042/0014, Red HERACLES), Ministerio de Economía y Competitividad (MEC) (SAF2012-31089 and SAF2015-69762-R), FEDER Funds and by the Asociación Española Contra el Cáncer (AECC). E.Á.'s lab is supported by the AECC, MEC-FEDER (RD12/0036/0017, PT13/0010/0056, RTC-2014-2102-1, ISCIII Sara Borrell CD06/00001, PI12/03102, PI14/01466), the European FP7 Projects EuroSARC (FP7-HEALTH-2011-two-stage, Project 278742 EUROSARC), Euroewing (FP7-HEALTH.2013.2.4.1-1, Project 602856), Fundación Memoria de DM Solorzano Barruso, Fundación Cris contra el Cáncer, Pablo Ugarte Foundation, and Fundación M. García Estrada. O.M.T. is funded by ISCIII-FEDER (CES12/021) and the AECC. AMC is funded by the European FP7 projects (FP7/2007-2013) under a Marie Curie International Reintegration Grant (PIRG-08- GA-2010-276998) and ISCIII-FEDER (CP13/00189). The Ewing group at the Developmental Tumor Biology Laboratory, Hospital Sant Joan de Déu, is supported by the AECC and the generous donations from Pablo Ugarte Foundation.

CONFLICTS OF INTEREST

Authors declare no competing financial interests.

REFERENCES

1. Delattre O, Zucman J, Plougastel B, Desmaze C, Melot T, Peter M, Kovar H, Joubert I, De Jong P, Rouleau G, Aurias A, and Thomas G. Gene fusion with an ETS DNA-binding domain caused by chromosome translocation in human tumours. *Nature*. 1992; 359: 162-5.
2. Sorensen PH, Lessnick SL, Lopez-Terrada D, Liu XF, Triche TJ, and Denny CT. A second Ewing's sarcoma translocation, t(21;22), fuses the EWS gene to another ETS-family transcription factor, ERG. *Nat Genet*. 1994; 6: 146-51.
3. Brohl AS, Solomon DA, Chang W, Wang J, Song Y, Sindiri S, Patidar R, Hurd L, Chen L, Shern JF, Liao H, Wen X, Gerard J, et al. The genomic landscape of the Ewing Sarcoma family of tumors reveals recurrent STAG2 mutation. *PLoS Genet*. 2014; 10: e1004475.
4. Crompton BD, Stewart C, Taylor-Weiner A, Alexe G, Kurek KC, Calicchio ML, Kiezun A, Carter SL, Shukla SA, Mehta SS, Thorner AR, de Torres C, Lavarino C, et al. The genomic landscape of pediatric Ewing sarcoma. *Cancer Discov*. 2014; 4: 1326-41.
5. Tirode F, Surdez D, Ma X, Parker M, Le Deley MC, Bahrami A, Zhang Z, Lapouble E, Grossetete-Lalami S, Rusch M, Reynaud S, Rio-Frio T, Hedlund E, et al. Genomic landscape of Ewing sarcoma defines an aggressive subtype with co-association of STAG2 and TP53 mutations. *Cancer Discov*. 2014; 4: 1342-53.
6. Riggi N, Knoechel B, Gillespie SM, Rheinbay E, Boulay G, Suva ML, Rossetti NE, Boonseng WE, Oksuz O, Cook EB, Formey A, Patel A, Gymrek M, et al. EWS-FLI1 utilizes divergent chromatin remodeling mechanisms to directly activate or repress enhancer elements in Ewing sarcoma. *Cancer Cell*. 2014; 26: 668-81.
7. Sankar S, Bell R, Stephens B, Zhuo R, Sharma S, Bearss DJ, and Lessnick SL. Mechanism and relevance of EWS/FLI-mediated transcriptional repression in Ewing sarcoma. *Oncogene*. 2013; 32: 5089-100.
8. Hancock JD, and Lessnick SL. A transcriptional profiling meta-analysis reveals a core EWS-FLI gene expression signature. *Cell Cycle*. 2008; 7: 250-6.
9. Richter GH, Plehm S, Fasan A, Rossler S, Unland R, Bennani-Baiti IM, Hotfilder M, Lowel D, von Luetichau I, Mossbrugger I, Quintanilla-Martinez L, Kovar H, Staeger MS, et al. EZH2 is a mediator of EWS/FLI1 driven tumor growth and metastasis blocking endothelial and neuroectodermal differentiation. *Proc Natl Acad Sci U S A*. 2009; 106: 5324-9.
10. de Napoles M, Mermoud JE, Wakao R, Tang YA, Endoh M, Appanah R, Nesterova TB, Silva J, Otte AP, Vidal M, Koseki H, and Brockdorff N. Polycomb group proteins Ring1A/B link ubiquitylation of histone H2A to heritable gene silencing and X inactivation. *Dev Cell*. 2004; 7: 663-76.
11. Wang H, Wang L, Erdjument-Bromage H, Vidal M, Tempst P, Jones RS, and Zhang Y. Role of histone H2A ubiquitination in Polycomb silencing. *Nature*. 2004; 431: 873-8.
12. Gao Z, Zhang J, Bonasio R, Strino F, Sawai A, Parisi F, Kluger Y, and Reinberg D. PCGF homologs, CBX proteins, and RYBP define functionally distinct PRC1 family complexes. *Mol Cell*. 2012; 45: 344-56.

13. Rai K, Akdemir KC, Kwong LN, Fiziev P, Wu CJ, Keung EZ, Sharma S, Samant NS, Williams M, Axelrad JB, Shah A, Yang D, Grimm EA, et al. Dual Roles of RNF2 in Melanoma Progression. *Cancer Discov.* 2015; 5: 1314-27.
14. Staeger MS, Hutter C, Neumann I, Foja S, Hattenhorst UE, Hansen G, Afar D, and Burdach SE. DNA microarrays reveal relationship of Ewing family tumors to both endothelial and fetal neural crest-derived cells and define novel targets. *Cancer Res.* 2004; 64: 8213-21.
15. Suh CH, Ordonez NG, Hicks J, and Mackay B. Ultrastructure of the Ewing's sarcoma family of tumors. *Ultrastruct Pathol.* 2002; 26: 67-76.
16. Cooper A, van Doorninck J, Ji L, Russell D, Ladanyi M, Shimada H, Krailo M, Womer RB, Hsu JH, Thomas D, Triche TJ, Spoto R, and Lawlor ER. Ewing tumors that do not overexpress BMI-1 are a distinct molecular subclass with variant biology: a report from the Children's Oncology Group. *Clin Cancer Res.* 2011; 17: 56-66.
17. Burdach S, Plehm S, Unland R, Dirksen U, Borkhardt A, Staeger MS, Muller-Tidow C, and Richter GH. Epigenetic maintenance of stemness and malignancy in peripheral neuroectodermal tumors by EZH2. *Cell Cycle.* 2009; 8: 1991-6.
18. Patel M, Simon JM, Iglesia MD, Wu SB, McFadden AW, Lieb JD, and Davis IJ. Tumor-specific retargeting of an oncogenic transcription factor chimera results in dysregulation of chromatin and transcription. *Genome Res.* 2012; 22: 259-70.
19. Bilke S, Schwentner R, Yang F, Kauer M, Jug G, Walker RL, Davis S, Zhu YJ, Pineda M, Meltzer PS, and Kovar H. Oncogenic ETS fusions deregulate E2F3 target genes in Ewing sarcoma and prostate cancer. *Genome Res.* 2013; 23: 1797-809.
20. Kauer M, Ban J, Kofler R, Walker B, Davis S, Meltzer P, and Kovar H. A molecular function map of Ewing's sarcoma. *PLoS One.* 2009; 4: e5415.
21. Douglas D, Hsu JH, Hung L, Cooper A, Abdueva D, van Doorninck J, Peng G, Shimada H, Triche TJ, and Lawlor ER. BMI-1 promotes ewing sarcoma tumorigenicity independent of CDKN2A repression. *Cancer Res.* 2008; 68: 6507-15.
22. Surface LE, Thornton SR, and Boyer LA. Polycomb group proteins set the stage for early lineage commitment. *Cell Stem Cell.* 2010; 7: 288-98.
23. Laezza F, Lampert A, Kozel MA, Gerber BR, Rush AM, Nerbonne JM, Waxman SG, Dib-Hajj SD, and Ornitz DM. FGF14 N-terminal splice variants differentially modulate Nav1.2 and Nav1.6-encoded sodium channels. *Mol Cell Neurosci.* 2009; 42: 90-101.
24. Burbidge SA, Dale TJ, Powell AJ, Whitaker WR, Xie XM, Romanos MA, and Clare JJ. Molecular cloning, distribution and functional analysis of the NA(V)1.6. Voltage-gated sodium channel from human brain. *Brain Res Mol Brain Res.* 2002; 103: 80-90.
25. Wittmack EK, Rush AM, Hudmon A, Waxman SG, and Dib-Hajj SD. Voltage-gated sodium channel Nav1.6 is modulated by p38 mitogen-activated protein kinase. *J Neurosci.* 2005; 25: 6621-30.
26. Wright MA, Mo W, Nicolson T, and Ribera AB. In vivo evidence for transdifferentiation of peripheral neurons. *Development.* 2010; 137: 3047-56.
27. Mohammadi M, McMahon G, Sun L, Tang C, Hirth P, Yeh BK, Hubbard SR, and Schlessinger J. Structures of the tyrosine kinase domain of fibroblast growth factor receptor in complex with inhibitors. *Science.* 1997; 276: 955-60.
28. Chen L, Sung SS, Yip ML, Lawrence HR, Ren Y, Guida WC, Sefti SM, Lawrence NJ, and Wu J. Discovery of a novel shp2 protein tyrosine phosphatase inhibitor. *Mol Pharmacol.* 2006; 70: 562-70.
29. Hadari YR, Kouhara H, Lax I, and Schlessinger J. Binding of Shp2 tyrosine phosphatase to FRS2 is essential for fibroblast growth factor-induced PC12 cell differentiation. *Mol Cell Biol.* 1998; 18: 3966-73.
30. Banasiak KJ, Burenkova O, and Haddad GG. Activation of voltage-sensitive sodium channels during oxygen deprivation leads to apoptotic neuronal death. *Neuroscience.* 2004; 126: 31-44.
31. Lessnick SL, and Ladanyi M. Molecular pathogenesis of Ewing sarcoma: new therapeutic and transcriptional targets. *Annu Rev Pathol.* 2012; 7: 145-59.
32. Koppens M, and van Lohuizen M. Context-dependent actions of Polycomb repressors in cancer. *Oncogene.* 2015; 35: 1341-52.
33. Ewing J. The Classic: Diffuse endothelioma of bone. *Proceedings of the New York Pathological Society.* 1921; 12:17. *Clin Orthop Relat Res.* 2006; 450: 25-27.
34. van der Schaft DW, Hillen F, Pauwels P, Kirschmann DA, Castermans K, Egbrink MG, Tran MG, Sciort R, Hauben E, Hogendoorn PC, Delattre O, Maxwell PH, Hendrix MJ, et al. Tumor cell plasticity in Ewing sarcoma, an alternative circulatory system stimulated by hypoxia. *Cancer Res.* 2005; 65: 11520-8.
35. Maniotis AJ, Folberg R, Hess A, Seftor EA, Gardner LM, Pe'er J, Trent JM, Meltzer PS, and Hendrix MJ. Vascular channel formation by human melanoma cells in vivo and in vitro: vasculogenic mimicry. *Am J Pathol.* 1999; 155: 739-52.
36. Aurora AB, Biyashev D, Mirochnik Y, Zaichuk TA, Sanchez-Martinez C, Renault MA, Losordo D, and Volpert OV. NF-kappaB balances vascular regression and angiogenesis via chromatin remodeling and NFAT displacement. *Blood.* 2010; 116: 475-84.
37. Javelaud D, and Besancon F. NF-kappa B activation results in rapid inactivation of JNK in TNF alpha-treated Ewing sarcoma cells: a mechanism for the anti-apoptotic effect of NF-kappa B. *Oncogene.* 2001; 20: 4365-72.
38. Lagirand-Cantaloube J, Laud K, Lilienbaum A, Tirode F, Delattre O, Auclair C, and Kryszke MH. EWS-FLI1 inhibits TNFalpha-induced NFkappaB-dependent transcription

- in Ewing sarcoma cells. *Biochem Biophys Res Commun*. 2010; 399: 705-10.
39. White DE, and Burchill SA. BAY 11-7082 induces cell death through NF-kappaB-independent mechanisms in the Ewing's sarcoma family of tumours. *Cancer Lett*. 2008; 268: 212-24.
 40. Sturla LM, Westwood G, Selby PJ, Lewis IJ, and Burchill SA. Induction of cell death by basic fibroblast growth factor in Ewing's sarcoma. *Cancer Res*. 2000; 60: 6160-70.
 41. Chotani MA, and Chiu IM. Differential regulation of human fibroblast growth factor 1 transcripts provides a distinct mechanism of cell-specific growth factor expression. *Cell Growth Differ*. 1997; 8: 999-1013.
 42. Xie Y, Zhou S, Chen H, Du X, and Chen L. Recent research on the growth plate: Advances in fibroblast growth factor signaling in growth plate development and disorders. *J Mol Endocrinol*. 2014; 53: T11-34.
 43. Calo V, Migliavacca M, Bazan V, Macaluso M, Buscemi M, Gebbia N, and Russo A. STAT proteins: from normal control of cellular events to tumorigenesis. *J Cell Physiol*. 2003; 197: 157-168.
 44. Behjati S, Basu BP, Wallace R, Bier N, Sebire N, Hasan F, and Anderson J. STAT3 Regulates Proliferation and Immunogenicity of the Ewing Family of Tumors In Vitro. *Sarcoma*. 2012; 2012: 987239.
 45. Lai R, Navid F, Rodriguez-Galindo C, Liu T, Fuller CE, Ganti R, Dien J, Dalton J, Billups C, and Khoury JD. STAT3 is activated in a subset of the Ewing sarcoma family of tumours. *J Pathol*. 2006; 208: 624-32.
 46. Jiang Y, Janku F, Subbiah V, Angelo LS, Naing A, Anderson PM, Herzog CE, Fu S, Benjamin RS, and Kurzrock R. Germline PTPRD mutations in Ewing sarcoma: biologic and clinical implications. *Oncotarget*. 2013; 4: 884-9. doi: 10.18632/oncotarget.1021.
 47. Aggarwal BB, Kunnumakkara AB, Harikumar KB, Gupta SR, Tharakan ST, Koca C, Dey S, and Sung B. Signal transducer and activator of transcription-3, inflammation, and cancer: how intimate is the relationship? *Ann N Y Acad Sci*. 2009; 1171: 59-76.
 48. Anderson JL, Titz B, Akiyama R, Komisopoulou E, Park A, Tap WD, Graeber TG, and Denny CT. Phosphoproteomic profiling reveals IL6-mediated paracrine signaling within the Ewing sarcoma family of tumors. *Mol Cancer Res*. 2014; 12: 1740-54.
 49. Yan S, Li Z, and Thiele CJ. Inhibition of STAT3 with orally active JAK inhibitor, AZD1480, decreases tumor growth in Neuroblastoma and Pediatric Sarcomas In vitro and In vivo. *Oncotarget*. 2013; 4: 433-45. doi: 10.18632/oncotarget.930.
 50. Ryland KE, Svoboda LK, Vesely ED, McIntyre JC, Zhang L, Martens JR, and Lawlor ER. Polycomb-dependent repression of the potassium channel-encoding gene *KCNA5* promotes cancer cell survival under conditions of stress. *Oncogene*. 2015; 34: 4591-600.
 51. Coles EG, Lawlor ER, and Bronner-Fraser M. EWS-FLI1 causes neuroepithelial defects and abrogates emigration of neural crest stem cells. *Stem Cells*. 2008; 26: 2237-44.
 52. Hu-Lieskovan S, Zhang J, Wu L, Shimada H, Schofield DE, and Triche TJ. EWS-FLI1 fusion protein up-regulates critical genes in neural crest development and is responsible for the observed phenotype of Ewing's family of tumors. *Cancer Res*. 2005; 65: 4633-44.
 53. Tirode F, Laud-Duval K, Prieur A, Delorme B, Charbord P, and Delattre O. Mesenchymal stem cell features of Ewing tumors. *Cancer Cell*. 2007; 11: 421-9.
 54. Cavazzana AO, Miser JS, Jefferson J, and Triche TJ. Experimental evidence for a neural origin of Ewing's sarcoma of bone. *Am J Pathol*. 1987; 127: 507-18.
 55. Franchi A, Pasquinelli G, Cenacchi G, Della RC, Gambini C, Bisceglia M, Martinelli GN, and Santucci M. Immunohistochemical and ultrastructural investigation of neural differentiation in Ewing sarcoma/PNET of bone and soft tissues. *Ultrastruct Pathol*. 2001; 25: 219-25.
 56. Rettig WJ, Garin-Chesa P, and Huvos AG. Ewing's sarcoma: new approaches to histogenesis and molecular plasticity. *Lab Invest*. 1992; 66: 133-7.
 57. Navarro S, Gonzalez-Devesa M, Ferrandez-Izquierdo A, Triche TJ, and Llombart-Bosch A. Scanning electron microscopic evidence for neural differentiation in Ewing's sarcoma cell lines. *Virchows Arch A Pathol Anat Histopathol*. 1990; 416: 383-91.
 58. Rorie CJ, Thomas VD, Chen P, Pierce HH, O'Bryan JP, and Weissman BE. The Ews/Fli-1 fusion gene switches the differentiation program of neuroblastomas to Ewing sarcoma/peripheral primitive neuroectodermal tumors. *Cancer Res*. 2004; 64: 1266-77.
 59. Teitell MA, Thompson AD, Sorensen PH, Shimada H, Triche TJ, and Denny CT. EWS/ETS fusion genes induce epithelial and neuroectodermal differentiation in NIH 3T3 fibroblasts. *Lab Invest*. 1999; 79: 1535-43.
 60. Olsen BR, Reginato AM, and Wang W. Bone development. *Annu Rev Cell Dev Biol*. 2000; 16: 191-220.
 61. Takashima Y, Era T, Nakao K, Kondo S, Kasuga M, Smith AG, and Nishikawa S. Neuroepithelial cells supply an initial transient wave of MSC differentiation. *Cell*. 2007; 129: 1377-88.
 62. Torchia EC, Jaishankar S, and Baker SJ. Ewing tumor fusion proteins block the differentiation of pluripotent marrow stromal cells. *Cancer Res*. 2003; 63: 3464-8.
 63. Kopen GC, Prockop DJ, and Phinney DG. Marrow stromal cells migrate throughout forebrain and cerebellum, and they differentiate into astrocytes after injection into neonatal mouse brains. *Proc Natl Acad Sci U S A*. 1999; 96: 10711-6.
 64. Woodbury D, Schwarz EJ, Prockop DJ, and Black IB. Adult rat and human bone marrow stromal cells differentiate into neurons. *J Neurosci Res*. 2000; 61: 364-70.
 65. Miyagawa Y, Okita H, Nakajima H, Horiuchi Y, Sato B, Taguchi T, Toyoda M, Katagiri YU, Fujimoto J, Hata J,

- Umezawa A, and Kiyokawa N. Inducible expression of chimeric EWS/ETS proteins confers Ewing's family tumor-like phenotypes to human mesenchymal progenitor cells. *Mol Cell Biol.* 2008; 28: 2125-37.
66. Riggi N, Suva ML, Suva D, Cironi L, Provero P, Tercier S, Joseph JM, Stehle JC, Baumer K, Kindler V, and Stamenkovic I. EWS-FLI-1 expression triggers a Ewing's sarcoma initiation program in primary human mesenchymal stem cells. *Cancer Res.* 2008; 68: 2176-85.
67. Tanaka M, Yamazaki Y, Kanno Y, Igarashi K, Aisaki K, Kanno J, and Nakamura T. Ewing's sarcoma precursors are highly enriched in embryonic osteochondrogenic progenitors. *J Clin Invest.* 2014; 124: 3061-74.
68. Cornaz-Buros S, Riggi N, DeVito C, Sarre A, Letovanec I, Provero P, and Stamenkovic I. Targeting cancer stem-like cells as an approach to defeating cellular heterogeneity in Ewing sarcoma. *Cancer Res.* 2014; 74: 6610-22.
69. Sohn EJ, Li H, Reidy K, Beers LF, Christensen BL, and Lee SB. EWS/FLI1 oncogene activates caspase 3 transcription and triggers apoptosis in vivo. *Cancer Res.* 2010; 70: 1154-63.
70. Torchia EC, Boyd K, Rehg JE, Qu C, and Baker SJ. EWS/FLI-1 induces rapid onset of myeloid/erythroid leukemia in mice. *Mol Cell Biol.* 2007; 27: 7918-34.
71. Lin PP, Pandey MK, Jin F, Xiong S, Deavers M, Parant JM, and Lozano G. EWS-FLI1 induces developmental abnormalities and accelerates sarcoma formation in a transgenic mouse model. *Cancer Res.* 2008; 68: 8968-75.
72. Martinez-Romero C, Rooman I, Skoudy A, Guerra C, Molero X, Gonzalez A, Iglesias M, Lobato T, Bosch A, Barbacid M, Real FX, and Hernandez-Munoz I. The epigenetic regulators Bmi1 and Ring1B are differentially regulated in pancreatitis and pancreatic ductal adenocarcinoma. *J Pathol.* 2009; 219: 205-13.
73. Riccardi C, and Nicoletti I. Analysis of apoptosis by propidium iodide staining and flow cytometry. *Nat Protoc.* 2006; 1: 1458-61.